ADVANCES IN ATMOSPHERIC SCIENCES, VOL. 22, NO. 4, 2005, 467–478

Future Projections of Precipitation Characteristics in East Asia Simulated by the MRI CGCM2

Akio KITOH, Masahiro HOSAKA, Yukimasa ADACHI, and Kenji KAMIGUCHI

Meteorological Research Institute, Tsukuba, 305-0052, *Japan*

(Received 29 October 2004; revised 22 February 2005)

ABSTRACT

Projected changes in precipitation characteristics around the mid-21st century and end-of-the-century are analyzed using the daily precipitation output of the 3-member ensemble Meteorological Research Institute global ocean-atmosphere coupled general circulation model (MRI-CGCM2) simulations under the Special Report on Emissions Scenarios (SRES) A2 and B2 scenarios. It is found that both the frequency and intensity increase in about 40% of the globe, while both the frequency and intensity decrease in about 20% of the globe. These numbers differ only a few percent from decade to decade of the 21st century and between the A2 and B2 scenarios. Over the rest of the globe (about one third), the precipitation frequency decreases but its intensity increases, suggesting a shift of precipitation distribution toward more intense events by global warming. South China is such a region where the summertime wet-day frequency decreases but the precipitation intensity increases. This is related to increased atmospheric moisture content due to global warming and an intensified and more westwardly extended North Pacific subtropical anticyclone, which may be related with an El Niño-like mean sea surface temperature change. On the other hand, a decrease in summer precipitation is noted in North China, thus augmenting a south-to-north precipitation contrast more in the future.

Key words: global warming, precipitation, GCM, East Asia

1. Introduction

It is expected that global warming will result in large changes in Asian climate, including changes in the monsoon intensity and duration over South Asia, Southeast Asia and East Asia, and even in the relationship between the El Niño-Southern Oscillation (ENSO) and the monsoon. An increase of the greenhouse gases will lead to increased surface air temperature and precipitation in the global mean sense, but its geographical distribution is not easy to project, in particular with respect to precipitation. IPCC (2001), which assessed the consistency of regional and seasonal mean precipitation change due to global warming among several models, reported that most tropical areas will have increased mean precipitation and most of the subtropical areas will have decreased mean precipitation at the end of the 21st century due to anthropogenic influence. An increase in summertime precipitation in East Asia and South Asia and a mean El Niño-like response in the tropical Pacific with a corresponding eastward shift of precipitation are also noted. Min et al. (2004) made East Asian climate change projections from multi-model ensembles, based on either simple arithmetic averages or skill-weighted averages. For annual mean climate changes, they showed an overall warmer and wetter climate in East Asia.

Climate change will have a seasonal dependency. With respect to model consistency about precipitation changes over the South Asia and East Asia regions, IPCC (2001) showed that the model projections are consistent in increased precipitation in JJA (June to August) but are inconsistent in DJF (December to February). Lal and Harasawa (2001), based on four relatively skillful model results, obtained a general increase in precipitation over most of Asia except for a decrease in summertime precipitation over Central Asia. Min et al. (2004) obtained that, for East Asia, the precipitation increases in the warmer season (April to September) while it decreases in the colder season (November to February). It is noted that wintertime inter-model uncertainty is larger than the signal.

Global warming would result in not only changes in mean precipitation but also in increases in the

*E-mail: kitoh@mri-jma.go.jp

amplitude and frequency of extreme precipitation events (e.g., Zwiers and Kharin, 1998; Kharin and Zwiers, 2000; Semenov and Bengtsson, 2002; Watterson and Dix, 2003). This would lead to more frequent floods and landslides with enormous damage on socio-economic sectors. A general drying of the mid-continental areas (IPCC, 2001) would lead to increases in summer droughts. Therefore more work has to be done for analysis of extreme events.

In this paper, we analyze changes in precipitation characteristics around the mid-21st century and end-of-the-century, using daily precipitation output projected by Meteorological Research Institute global ocean-atmosphere coupled general circulation model (MRI-CGCM2) simulations under the Special Report on Emissions Scenarios (SRES) A2 and B2 scenarios. We analyze total precipitation, wet-day frequency and precipitation intensity with emphasis on those changes over East Asia.

2. Model and experiment

The model used is the global ocean-atmosphere coupled GCM called MRI-CGCM2 (Yukimoto et al., 2001). The atmospheric component of the model (AGCM) has been developed based on a version of the operational weather forecasting model of the Japan Meteorological Agency (JMA). The horizontal resolution is T42 in wave truncation (about 2.8° by 2.8° grid spacing in longitude and latitude). The vertical configuration consists of a 30-layer sigma-pressure hybrid coordinate with the top at 0.4 hPa. Some of the physical process schemes are replaced with those of the original JMA version. Details of the AGCM are described in Shibata et al. (1999).

The oceanic component of the model is a Bryan-Cox type ocean general circulation model (OGCM) with a global domain. The horizontal grid spacing is 2.5° in longitude and 2.0° in latitude. Between 4°S and 4°N, the meridional grid spacing is set to 0.5° in order to have a good resolution for the equatorial oceanic waves. There are 23 vertical levels where the uppermost layer has a 5.2 m thickness. An eddy isopycnal mixing scheme is used in addition to sub-grid mixing using viscosities and diffusivities. Solar radiation penetrates seawater with an absorptivity of 10-m-depth e-folding decay, which heats several tens of meters of surface seawater.

We conducted first a historical simulation for 1850–2000 with observed atmospheric greenhouse gas concentrations and aerosols, solar variations and volcanic forcing (historical run) and then future projections up to 2100 under the SRES A2 and B2 scenarios (IPCC, 2000). Three ensemble runs were performed for each scenario from different initial conditions. Ashrit et al. (2005) investigated the impact of global warming on the Indian summer monsoon and the ENSO-monsoon teleconnection of this experiment, and found an increase of South Asian summer monsoon rainfall, fluctuations of interannual variability of monsoon rainfall and a weakening of the ENSO-monsoon relationship toward the end of the 21st century.

In this paper, we compare the precipitation characteristics (total precipitation, wet-day frequency and intensity) in the 3-member ensemble averages at the mid-21st century (2041–2060) and at the end of the 21st century (2081–2100) under the SRES-A2 and B2 scenarios with the 3-member ensemble averages of the present-day (1981-2000) simulations of the historical run.

3. Results

3.1 *Model climate*

Yukimoto et al. (2001) described the model climate in general. The model performance in simulating the summer monsoon climate over South Asia, East Asia and the western North Pacific is reported by Rajendran et al. (2004). The model simulates many climatological features of the summer monsoon rainfall and its associated circulation fields, including the seasonal mean monsoon precipitation and circulation in its magnitude and flow pattern, seasonal variation, climatological monsoon onset, and sub-seasonal variations.

Validation of the simulated wet-day frequency and intensity has rarely been reported, probably due to the absence of reliable global gridded data of a long duration. Kamiguchi et al. (2004) evaluated the daily precipitation characteristics simulated by MRI AGCM, which is an atmospheric part of the current coupled model, by using gamma distribution parameters. They showed that the MRI AGCM underestimated intensity and overestimated wet-day frequency in low latitudes, but concluded that the model has sufficient ability to simulate daily precipitation characteristics due to a good correlation with observations on the whole. Here we compare the observed and simulated annual precipitation characteristics in total precipitation, wet-day frequency (threshold of 1 mm d^{-1}) and precipitation intensity on wet-days (Fig. 1). For validation we used the Global Precipitation Climatology Project (GPCP) one-degree daily data for the period 1998–2002 (Huffman et al. 2001). The model data are derived for the period 1981–2000 of the 3-member historical run. Simulated total precipitation is in accord with the observation in its spatial distribution

and magnitude. Simulated annual global mean precipitation is 3.02 mm d^{-1}, which is 13% larger than the GPCP climatology (2.67 mm d^{-1}). The model overestimated wet-day frequency by 47% (0.30 in GPCP and 0.44 in GCM for the global mean value), while it underestimated the intensity by 25% (8.35 vs 6.30 mm d^{-1}, respectively). Thus the overestimation of frequency and the underestimation of intensity cancel out each other resulting in a reasonable amount for total precipitation. A large difference can be found in the Tropics, implying a more constant occurrence of cumulus convection in the model. Although they look different from each other, these values have not been evaluated in the past, probably due to uncertainty in global daily precipitation data. Quantitative evaluation needs further analysis using multiple observation data sources. Although different in magnitude, similar spatial distributions both in wet-day frequency and intensity between the model and the observation would enable us to use the model precipitation characteristics at least in qualitative discussions.

3.2 *Annual mean changes*

In the scenario experiments, the model simulates an overall global warming while its rate depends on the scenario used. Figure 2 shows the time series of the annual and global mean surface air temperature and precipitation of the historical run and the A2 and B2 scenario runs. The averages of three ensemble runs are shown. The annual mean temperature indicates a

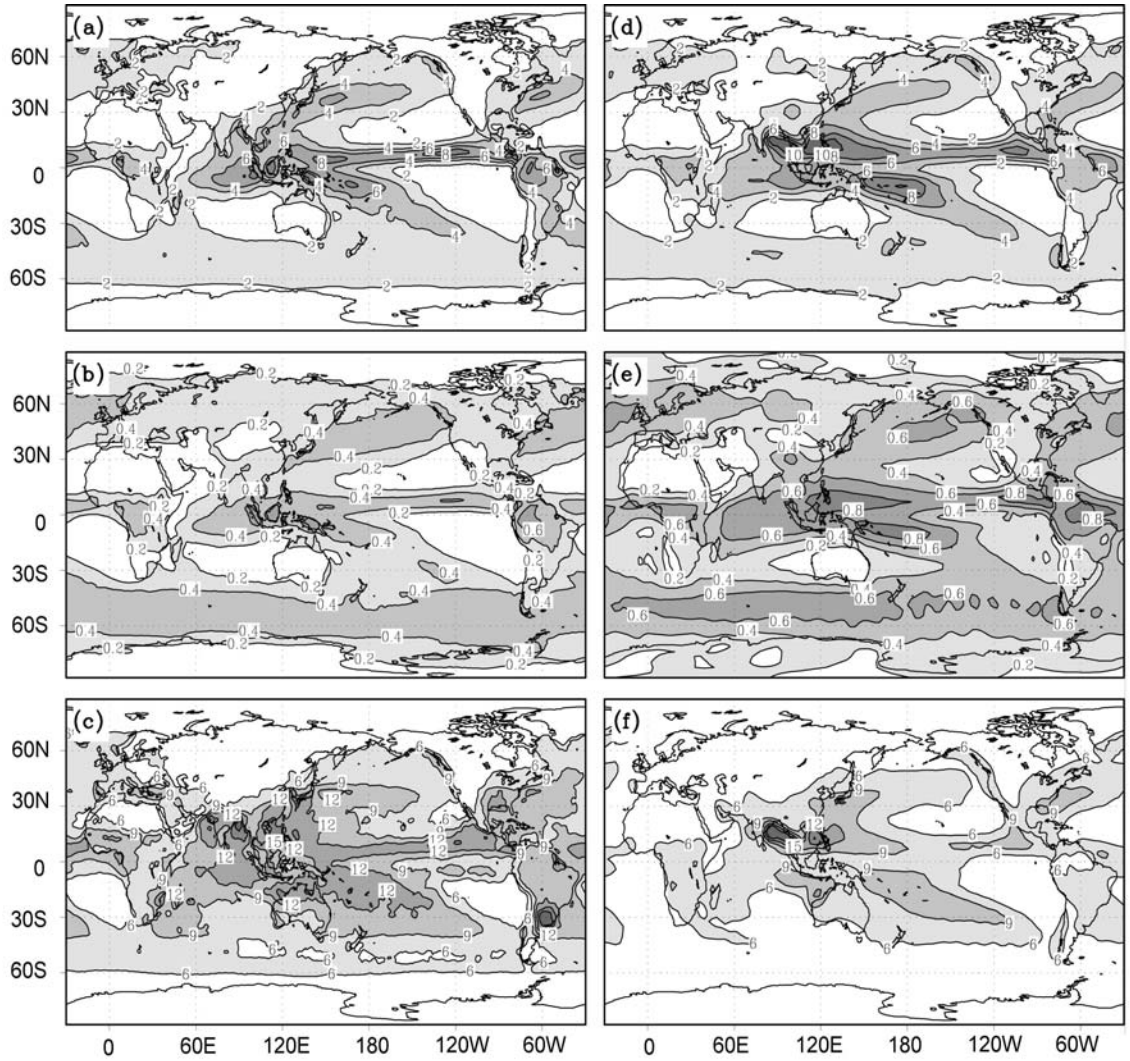

Fig. 1. (a–c) Observed annual precipitation characteristics using the GPCP data (Huffman et al., 2001). (a) Total precipitation (units: mm d^{-1}), (b) Wet-day frequency with a threshold of 1 mm d^{-1} (units: fraction), (c) Precipitation intensity on wet days (units: mm d^{-1}). (d–f) As in (a–c) except for the model simulation for 1981–2000 of the historical run.

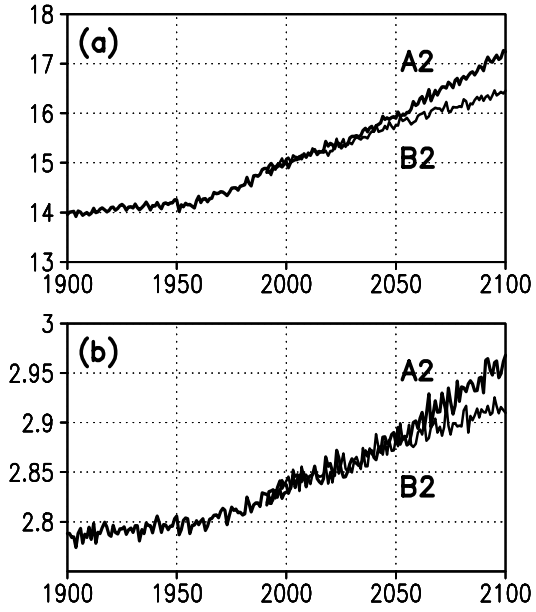

Fig. 2. Time series of annual and global mean (a) surface air temperature (K) and (b) precipitation (mm d^{-1}) of the historical and the SRES-A2 and B2 scenario runs. Averages of 3 ensemble integrations are shown.

strong warming trend particularly towards the late 21st century in the SRES-A2 scenario to attain a warming of 2.19 K at 2100 compared to the present (1981–2000 of the historical run). In the SRES-B2 scenario the warming is less (1.40 K) due to differences in the greenhouse gas concentration scenario. However, the difference in the warming in the mid-21st century is small between A2 (0.84 K) and B2 (0.72 K); the scenario dependence becomes larger after around the 2050s. Changes in the annual mean precipitation show an increase of 4.54% in the SRES-A2 scenario, while they show an increase of 2.48% in the B2 scenario at 2100. Again the differences between the A2 and B2 scenarios are very small until the mid-21st century (1.41% and 1.57%, respectively).

Figure 3 shows the change in annual mean surface air temperature during 2041–2060 and 2081–2100 for both the A2 and B2 scenarios from the 1981–2000 averages of the historical run. Strong warming is evident in the high latitudes at the end of the 21st century in the SRES-A2 scenario. However the spatial patterns are similar to each other between the different scenario runs and also between the different periods, with the higher latitudes showing a larger warming than the lower latitudes, and the land surface showing a larger warming than over the oceans. These features are similar to the other model results reported in IPCC (2001). It is noted that over the tropical Pacific, the temperature in the eastern part warms up more than in the western part. This suggests that the long-term

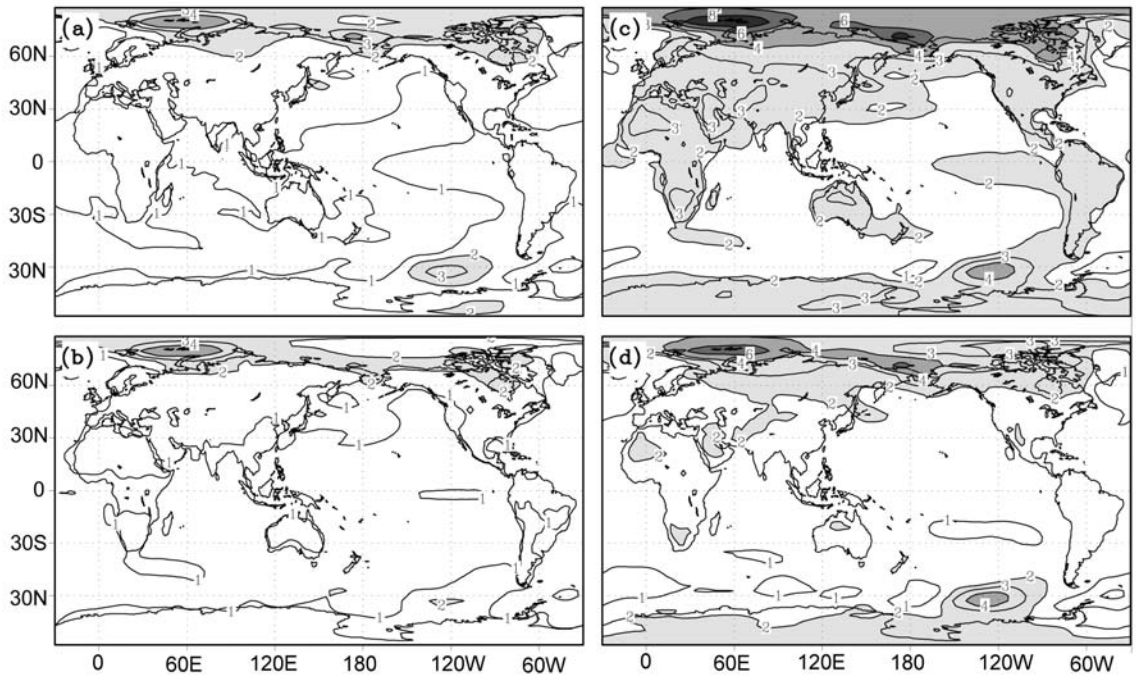

Fig. 3. Annual mean surface air temperature difference (future minus present) in K during (a) 2041–2060 for A2, (b) 2041–2060 for B2, (c) 2081–2100 for A2, and (d) 2081–2100 for B2. The difference is calculated from the 1981–2000 mean of the historical run.

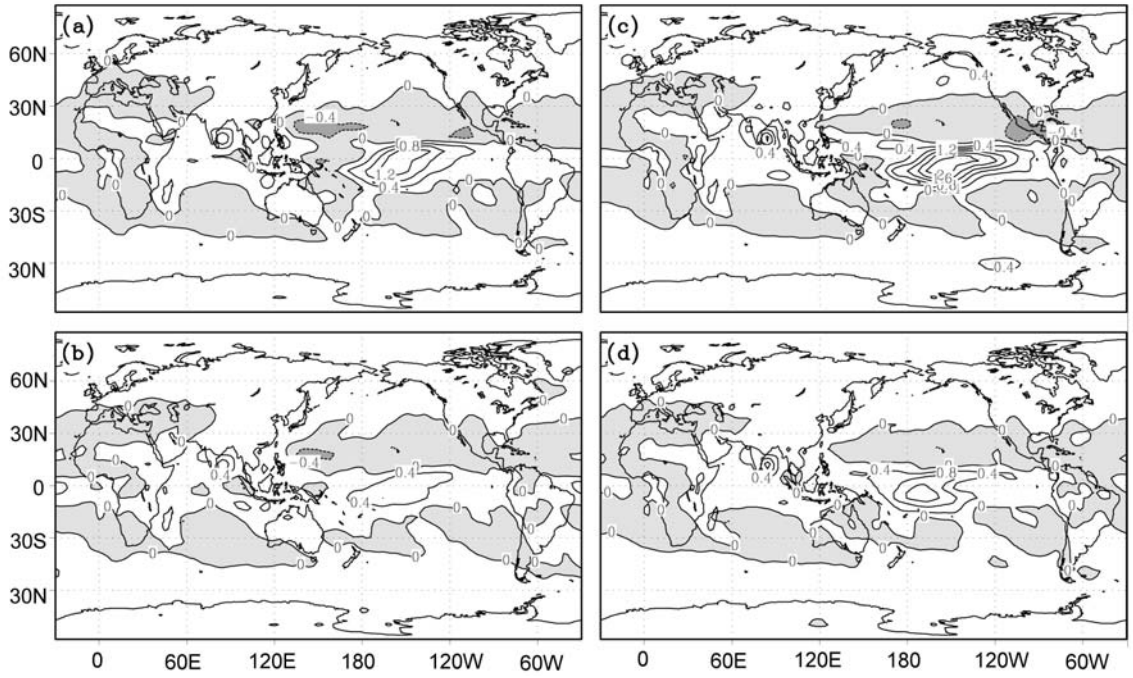

Fig. 4. As in Fig. 3 except for total precipitation. The contour interval is 0.4 mm d^{-1}.

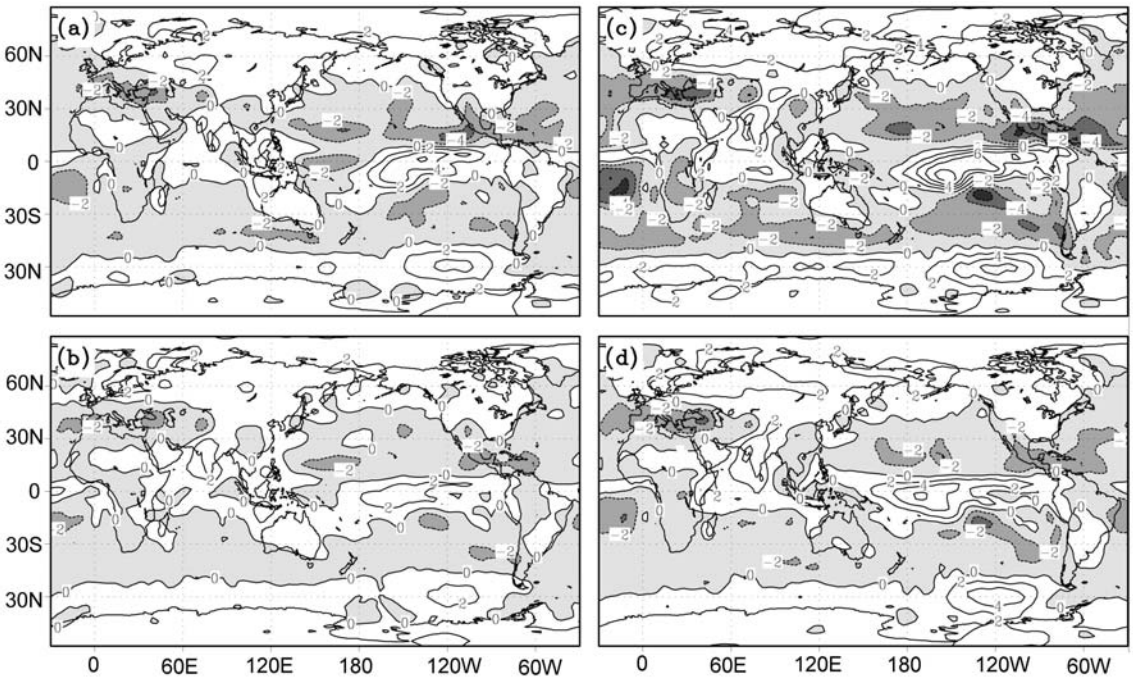

Fig. 5. As in Fig. 3 except for wet-day frequency. The contour interval is 2%.

mean Pacific change by global warming resembles an El Niño-like pattern (SST figure not shown). This El Niño-like mean base state is similar to what is projected by many models (IPCC, 2001).

Figure 4 shows the change in annual mean total precipitation during 2041–2060 and 2081–2100 for both the A2 and B2 scenarios. In the tropical Pacific region, an eastward displacement of the major precipitation center is noted, associated with El Niño-like background SST changes. In Asia, the annual

mean precipitation increased in both scenarios and in both time periods. The model showed an increased rainfall in the South Asian summer monsoon (Ashrit et al., 2005). In higher latitudes, total precipitation increased, while there was a decrease in precipitation over the subtropical oceans, particularly over the North Pacific subtropical region and the Mediterranean region. The overall pattern of annual mean precipitation changes is similar to that of the ensemble means of several models reported in IPCC (2001). Georgi et al. (2001) compared model consistency of seasonal mean precipitation change, and found that the models with the SRES-A2 scenario are consistent in increased precipitation in JJA, but are inconsistent in DJF over the South Asia and East Asia regions.

3.3 *Changes in precipitation frequency and intensity*

To project future precipitation changes, one needs to investigate not only the total precipitation changes but also the changes in frequency, intensity and other statistics such as extremes (e.g., Semenov and Bengtsson, 2002; Watterson and Dix, 2003). In this paper, we compare changes in wet-day frequency and intensity. Figure 5 shows the changes in annual wet-day frequency during 2041–2060 and 2081–2100 for the A2 and B2 scenarios. Here we define the day as rainy (a wet-day) when daily precipitation is greater than or equal to 1.0 mm d^{-1}. The overall spatial pattern of wet-day frequency change is similar to that of total precipitation change, but relatively large changes in wet-day frequency can be found in the middle and high latitudes. Also the area extent of negative changes in wet-day frequency (less rainy days in the future) is broader than the area of negative changes in total precipitation. Less frequent rainy days in the future is evident over the Mediterranean region as well as over the subtropical oceans. Over Asia, increased wet-day frequency in India is contrasted with decreased wet-day frequency in southern China. Again these features appear even in the mid-21st century, and become larger in magnitude as the warming becomes greater.

Figure 6 shows the changes in the intensity of precipitation or the simple daily intensity index that is defined as the annual total precipitation divided by the number of rainy days greater than or equal to 1 mm d^{-1}. The overall pattern is again similar to Figs. 4 and 5 in the Tropics and high latitudes. However, in the mid-latitudes, there are regions with opposite signs of changes between intensity and frequency. For example, over southern China, the change in frequency is negative while the change in intensity is positive. This is also the case for the Mediterranean region. The area extent where the intensity has decreased is relatively small. If the area extent of positive or negative changes is compared, total precipitation has increased over about 65% of the globe during 2081–2100 in the SRES-A2 scenario (Fig. 4c). We find 42% of the globe

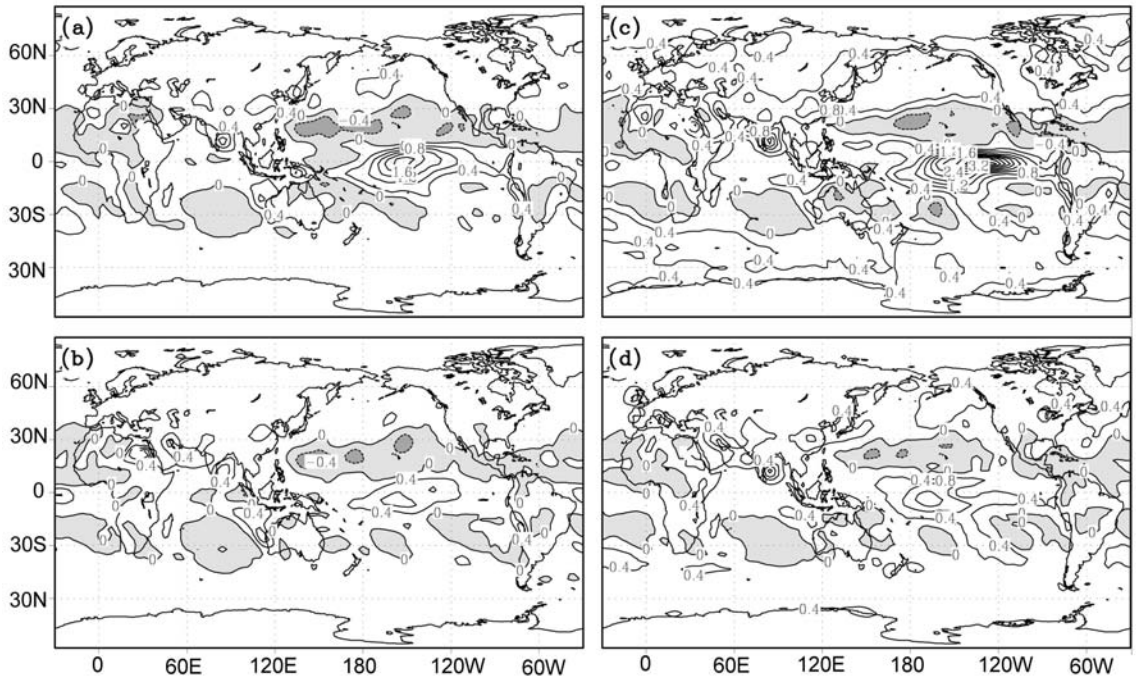

Fig. 6. As in Fig. 3 except for precipitation intensity on wet day. The contour interval is 0.4 mm d^{-1}.

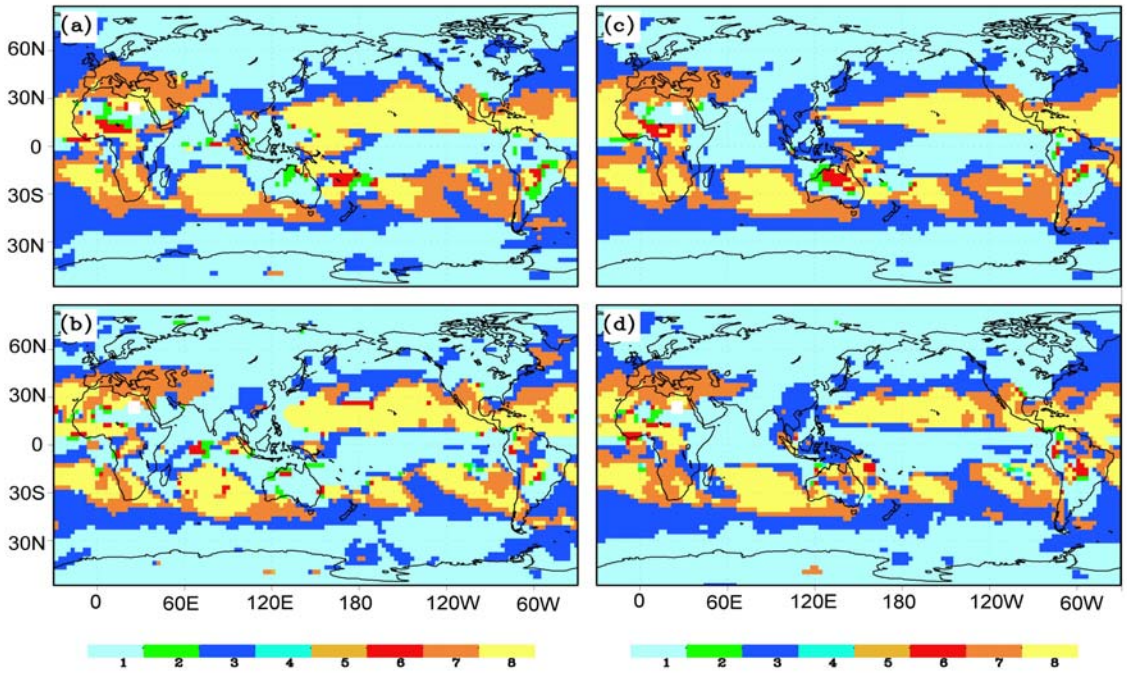

Fig. 7. Changes in three characteristics in precipitation based on total precipitation (T), wet-day frequency (F) and precipitation intensity of wet days (I). Classification of types 1–8 are + + +, ++ –, + – +, + – –, – + +, – + –, – – +, and – – – for T, F, I, respectively. (a) 2041–2060, A2; (b) 2041–2060, B2; (c) 2081–2100, A2; (d) 2081–2100, B2.

where the wet-day frequency has increased (Fig. 5c), while we find 79% where the intensity of precipitation on rainy days has increased (Fig. 6c). These numbers differ by only a few percent from decade to decade and between the A2 and B2 scenarios in this model, but they could differ from model to model.

In order to investigate the relationship among the above three characteristics, we classified all the grid points into 8 categories. Figure 7 shows the changes in three characteristics in precipitation based on total precipitation (T), wet-day frequency (F) and wet-day precipitation intensity (I). Grid points where changes in sign of T, F and I with $+++, ++-, +--, +--, -++, -+-, --+$, and $---$ are defined as types 1, 2, 3, 4, 5, 6, 7 and 8, respectively. From the figure, it is revealed that the overall patterns of the classification are very similar to each other between the two scenario runs and also between the two time periods. Table 1 shows the area ratio of each type. It should be noted that types 5 and 6 appeared because we set a criterion of 1 mm d^{-1} for the wet-day definition. It is shown that both the frequency and intensity increased in about 40% of the globe (type 1), while both the frequency and intensity decreased in about 20% of the globe (type 8). In between, which occupies around one third of the globe, the precipitation frequency decreased but its intensity increased (type 3 or 7). The existence of types 3 and 7 suggests a climate shift toward more intense precipitation events by global warming. Moreover, the ratios of types 3 and 7 become larger from the SRES-B2 scenario to the SRES-A2 scenario, and also from the period of 2041–2060 to the period 2081–2100, corres-

Table 1. Relative area ratio (% of the globe) of 8 classifications for the middle (2041–2060) and the end (2081–2100) of the 21st century for the SRES-A2 and B2 scenario runs. Types 2, 4, 5 and 6 are grouped into one category in this Table.

	Total	Frequency	Intensity	A2/2041–2060	A2/2081–2100	B2/2041–2060	B2/2081-2100
Type 1	+	+	+	41.46	39.48	45.95	41.47
Type 3	+	–	+	21.80	25.66	20.15	25.06
Type 7	–	–	+	14.83	16.04	12.64	14.62
Type 8	–	–	–	18.72	16.50	18.59	16.88
Others				3.19	2.32	2.67	1.97

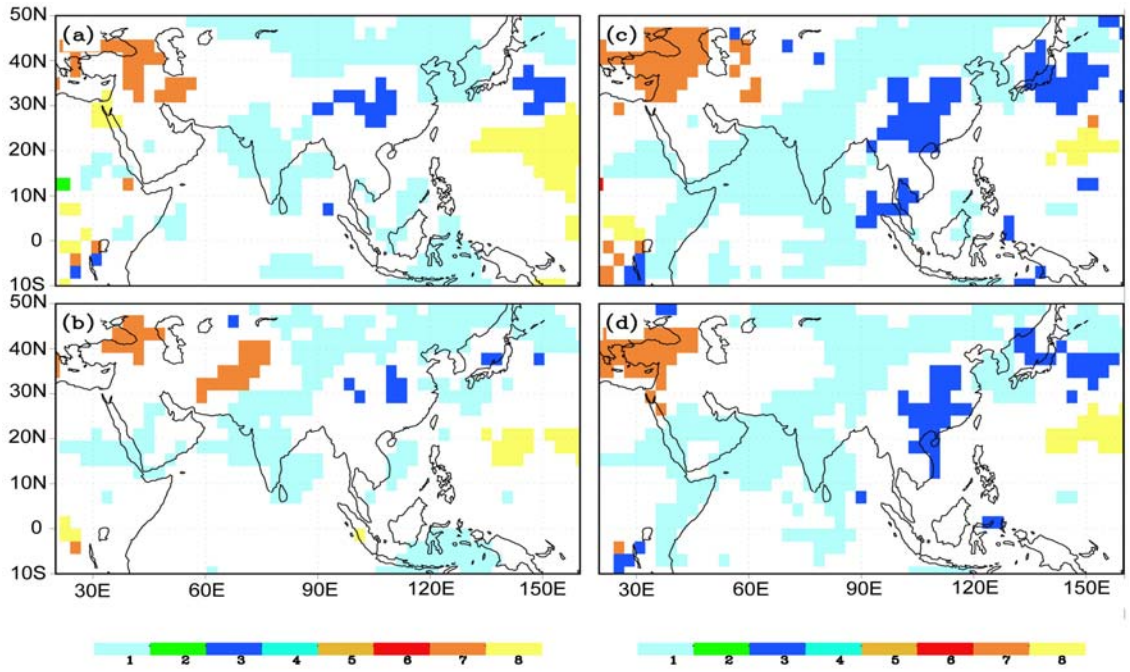

Fig. 8. As in Fig. 7 except for the Asian region, and only grid points where the 3 ensemble members are consistent are plotted.

ponding to an increasing magnitude of warming.

The Mediterranean and the Middle East is categorized as a type 7 region where both the total precipitation and number of rainy days decreased but precipitation intensity increased. It is interesting to note that the observed rainfall over the Mediterranean showed an increase of extreme rainfall in spite of a decrease in total precipitation (e.g., Alpert et al., 2002).

The analyses above are performed based on the ensemble averages of three member integrations to reduce internal variability (noise). In order to assess how each ensemble member is different from the others and how robust the above result is, we mask out the grid points where the ensemble members differ on categorized classifications. Figure 8 shows the changes in the three characteristics of precipitation based on total precipitation, wet-day frequency and wet-day precipitation intensity over Asia, but only the grid points are plotted where all the three ensemble members are consistent. As was anticipated, the signal becomes more robust as the global warming becomes larger and the number of grid points with inter-ensemble consistency becomes greater. Also the results of the SRES-A2 and SRES-B2 scenarios become similar to each other in 2081-2100. They show the type-3 response (less wet-day frequency, more intense precipitation, and more total precipitation) in East Asia and Southeast Asia, particularly over South China and some parts of Japan. This area is contrasted with the type-1 area (more wet-day frequency, more intense precipitation, and more total precipitation), in which India, Korea and the western part of Japan are included.

3.4 *Seasonal changes over China*

In the previous sub-section we showed that East Asia and Southeast Asia are type-3 regions and may be considered as two of the more flood vulnerable regions in the future climate. These analyses are performed on the annual mean changes, but changes in precipitation characteristics may differ from season to season. Therefore the seasonal change of precipitation characteristics is now investigated. Figure 9 compares the seasonal changes of total precipitation, wet-day frequency and precipitation intensity averaged for South China (26°–33°N, 100°–120°E) for the present (1981–2000) and the period 2081–2100 of the SRES-A2 scenario run. When the difference between the future and present is statistically significant at the 90% level, black boxes are plotted on the abscissa when the future is larger than the present or by a lighter shade when the future is smaller than the present. The model projection shows some decrease in the wet-day frequency in the mid-summer season of May–August (Fig. 9b), but the precipitation intensity increases almost all the year round (Fig. 9c). The total precipitation increases

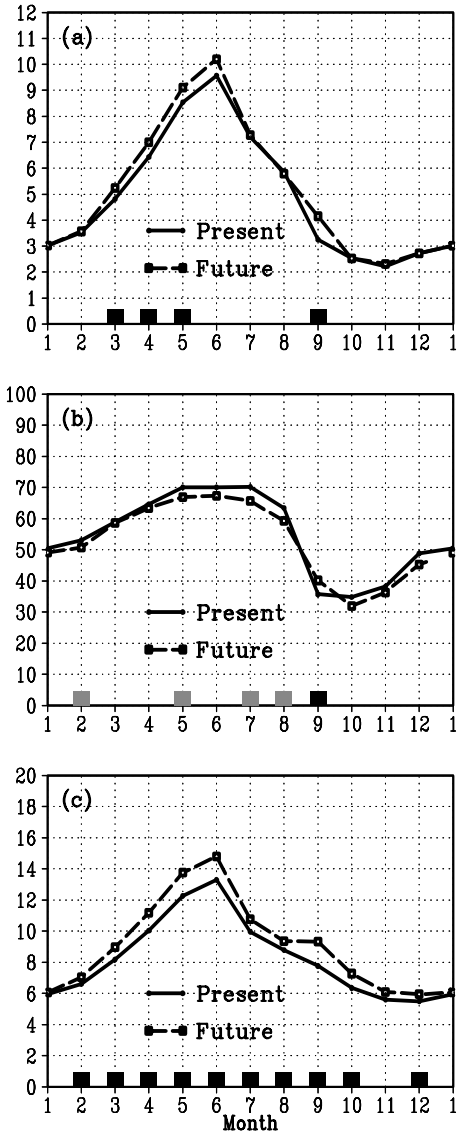

Fig. 9. Seasonal changes of (a) total precipitation (units: mm d^{-1}), (b) wet-day frequency (units: %) and (c) precipitation intensity (units: mm d^{-1}) for South China (26°–33°N, 100°–120°E). A solid line denotes the present and a dashed line denotes 2081–2100 for the SRES-A2 scenario run. Boxes are plotted along the abscissa where the difference between the future and present is statistically significant at the 90% level based on 3 ensemble members, where a black (light) box denotes that the future is larger (smaller) than the present.

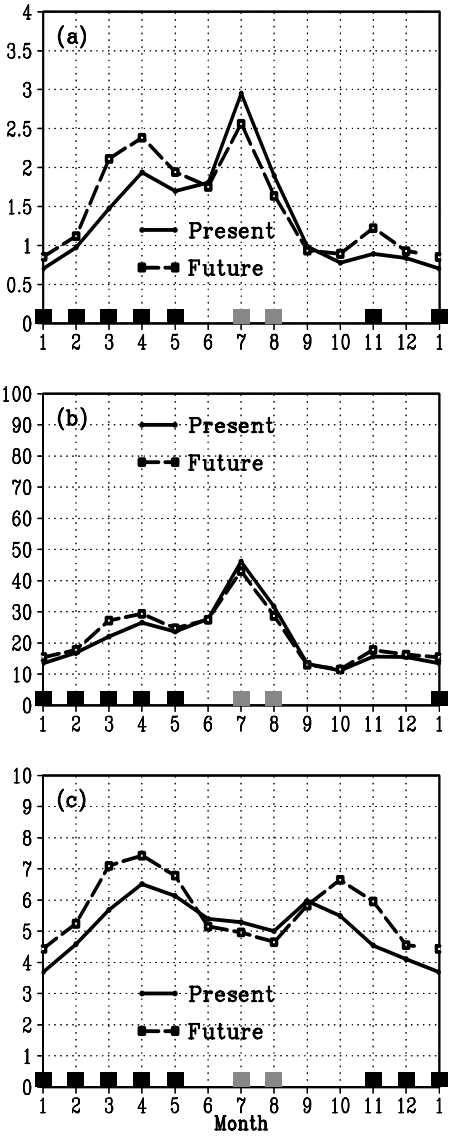

Fig. 10. As in Fig. 9 except for North China (35°–45°N, 100°–120°E).

in the early rainy season of March–May, which is attributed to more intense rainfall despite a decrease in rainy events.

Changes in seasonal precipitation characteristics in North China show a very different behavior than in South China. Figure 10 compares the seasonal changes of the total precipitation, wet-day frequency and precipitation intensity averaged for North China (35°–45°N, 100°–120°E) for the present and for the period 2081–2100 of the SRES-A2 scenario run. In this region, both the frequency and intensity decrease in summer and increase in winter and spring. Thus the total precipitation shows the same seasonal change with a decrease in summer and an increase in winter and spring. It is noted that changes in intensity contribute more than changes in frequency to the total precipitation changes.

Figure 11 shows the frequency distribution of precipitation intensity in the June–August (JJA) season for the South China and North China regions for the present (1981–2000) and 2081–2100 periods for the

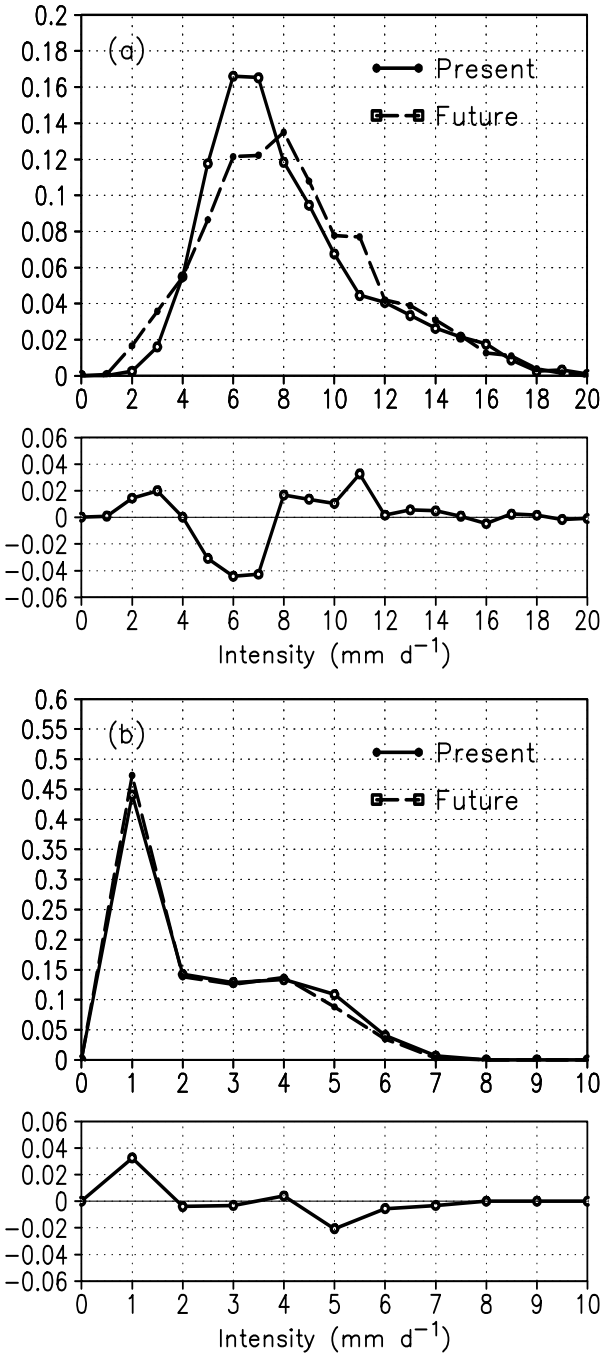

Fig. 11. Frequency distribution of precipitation intensity in the June–August (JJA) season for (a) South China (26°–33°N, 100°–120°E) and (b) North China (35°–45°N, 100°–120°E). A solid line denotes the present and a dashed line denotes 2081–2100 for the SRES-A2 scenario run. Bottom panels show the difference (future minus present). An intensity of 0 denotes no precipitation, 1 denotes 0–1 mm d^{-1}, 2 denotes 1–2 mm d^{-1}, and so on.

SRES-A2 scenario run. Here, an intensity of 0 denotes no precipitation, 1 denotes 0–1 mm d^{-1}, 2 denotes 1–2 mm d^{-1}, and so on. In South China, there is a maximum around 6–7 mm d^{-1} in the control run. Both the mean and standard deviation increase in the future climate, with a greater probability of occurrence for precipitation intensity in the ranges of more than 700 mm season^{-1} (greater than 8 mm d^{-1}) and less than 300 mm season^{-1} (less than 3 mm d^{-1}) in the A2 scenario experiment in this region. On the other hand, the probability of moderate-strength precipitation with an intensity of 5–7 mm d^{-1} decreases. This model result suggests that more extreme events of either flood or drought may occur due to global warming in this region. North China has a different pdf pattern with the largest frequency in the weakest intensity range of less than 1 mm d^{-1}. A decrease in summer precipitation and an increase in winter precipitation in this region are shown in Fig. 10. Figure 11b shows that this summertime decrease is mainly due to a decrease of relatively strong (greater than 5 mm d^{-1}) precipitation in North China.

In order to interpret the large contrast of changes in precipitation characteristics between the South China and North China regions, the moisture flux fields are investigated. Figure 12 shows the June-August (JJA) total moisture flux and its convergence in the model present-day climate (1981–2000 of the historical run) and its changes in 2081–2100 of the SRES-A2 scenario run. There is a moisture flux convergence over a wide area in Asia. Increased atmospheric moisture content in the warmer air in the scenario run leads to larger moisture flux and increased precipitation (e.g., Kitoh et al., 1997; Ashrit et al., 2005). It is also noted that the Pacific subtropical anticyclone becomes stronger and more southerly moisture flux converges over South China (Fig. 12b). It is plausible that wet-day frequency decreases due to a westward shift and an intensification of the subtropical anticyclone while larger moisture flux results in more intense precipitation when the event occurs. Moisture flux convergence is also larger over Japan, suggesting more intense Baiu activity in this region. In a warmed climate, the Baiu withdrawal date becomes late in this model, but this topic of Baiu rainfall will be reported elsewhere.

Precipitation variations in this region are affected by many factors including tropical SST anomalies, the subtropical anticyclone variability, the Pacific-Japan teleconnection pattern, the tropical intraseasonal oscillation, variability over the Eurasian continent and the Southern Hemisphere circulation (e.g., Huang and Wu, 1989; Nitta and Hu, 1996; Kawamura, 1998; Xue et al., 2004). The impact of the ENSO cycle on the East Asian summer monsoon has been investigated by many authors. For example, Huang et al. (2004) reviewed that, during the developing stage of El Niño,

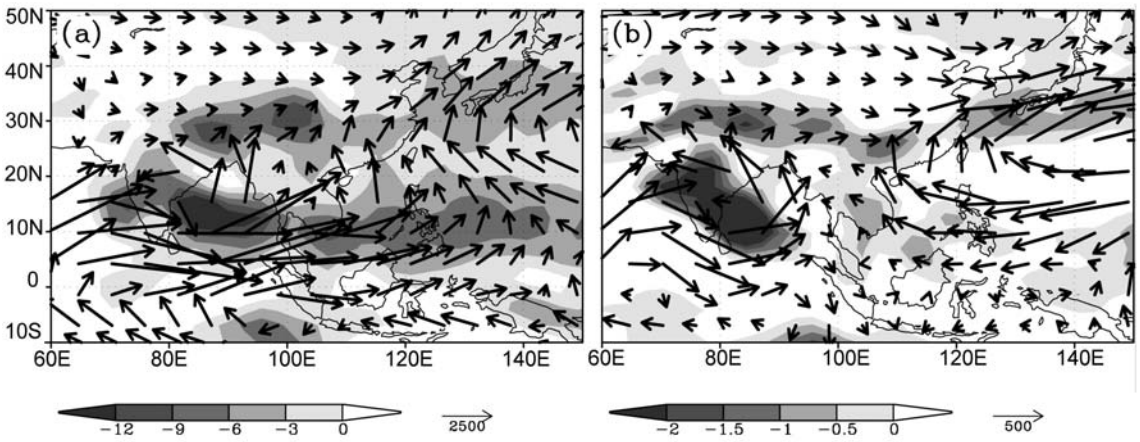

Fig. 12. (a) Total moisture flux and its divergence in JJA for the period 1981–2000 of the historical run. The shaded areas denote moisture flux convergence. (b) Changes in total moisture flux and its divergence in JJA for the period 2081–2100 of the SRES-A2 scenario run.

above normal rainfall occurs over South China through Japan, while drought conditions tend to occur in North China. The circulation anomalies obtained in the model future world (Fig. 12b) are similar to what are often observed at times of El Niño events (Zhang et al., 1996), and thus the simulated El Niño-like mean climate response in the tropical Pacific (Figs. 3 and 4) may be related to these changes in East Asian climate.

4. Summary and discussion

In this paper, the daily precipitation data produced by the MRI-CGCM ensemble runs under the SRES–A2 and SRES-B2 scenarios are analyzed. In the Tropics, an eastward displacement of precipitation was noted, associated with El Niño-like mean SST changes. From the analysis of precipitation characteristics around the middle and end of the 21st century compared to the end of the 20th century (1981–2000), it is found that over one third of the globe, the number of rainy days decreases but precipitation intensity increases. The area extent of there regions increases towards the end of the 21st century due to the enhanced warming. South China is a region where summertime wet-day frequency decreases but precipitation intensity increases. This is related to increasing atmospheric moisture content and an intensified and westward-extended North Pacific subtropical anticyclone that transports more moisture from the south into China. This circulation change may be associated with El Niño-like mean SST changes, although other possibilities remain. On the other hand, a decrease in summer precipitation is noted in North China, thus augmenting a greater south-to-north precipitation contrast in the future than the already-existing contrast. The observed characteristic of summer precipitation in China shows a drying trend in the north and a wetting trend in the central part during the 1951–2000 period (Hu et al., 2003).

This north-south contrast of summertime precipitation anomaly (northern drought and southern flood) is a characteristic feature of our model. Bueh et al. (2003), on the other hand, reported that the ECHAM4/OPYC3 GCM showed an increased precipitation in North China all year round. The multi-model ensemble results by Min et al. (2004) also showed that precipitation increases over all of East Asia in summer. Thus our model result of decreased precipitation in summer in North China is contrary to their results. Hu et al. (2003) noticed large uncertainties among the models in simulating future precipitation changes. The reason for the inter-model discrepancy should be examined further.s

Changes in extreme precipitation events, other than wet-day frequency and intensity, should also be investigated (e.g., Watterson and Dix, 2003). However it is also true that the current global climate models have limitations in terms of spatial resolution. In this paper, we used the T42 (about 280-km) resolution model, and it would be very difficult to diagnose extreme events with these coarse resolution models. In order to discuss particular extreme events, how much spatial resolution is needed should be elaborated upon. We at MRI have developed a very-high spatial resolution (20-km mesh) atmospheric GCM and made a time-slice experiment for the present and future of 20-years each together with other resolution models. Such a result will be reported elsewhere in the near future.

Acknowledgments. The authors acknowledge S. Yukimoto for the MRI-CGCM2 historical and scenario ex-

periments. This research was partly funded by the "Study of the Prediction of Regional Climate Changes over Japan due to Global Warming" project (FY2000-FY2004) of the Japan Meteorological Agency (JMA) and by the "Water Resource and Its Variability in Asia in the 21st Century" project (FY2001-FY2003) of the "Special Coordination Funds for Promoting Science and Technology" of the Ministry of Education, Culture, Sports, Science and Technology (MEXT).

REFERENCES

Alpert, P., and Coauthors, 2002: The paradoxical increase of Mediterranean extreme daily rainfall in spite of decrease in total values. *Geophys. Res. Lett.*, **29**, 10.1029/2001GL013554.

Ashrit, R., S. Yukimoto, and A. Kitoh, 2005: Transient response of ENSO-monsoon teleconnection in MRI-CGCM2.2 climate change simulations. *J. Meteor. Soc. Japan*, **83**, 273–291.

Bueh, C., U. Cubasch, Y. Lin, and L. Ji, 2003: The change of North China climate in transient simulations using the IPCC SRES A2 and B2 scenarios with a coupled atmosphere-ocean general circulation model. *Adv. Atmos. Sci.*, **20**, 755–766.

Giorgi, F., and Coauthors, 2001: Emerging patterns of simulated regional climatic changes for the 21st century due to anthropogenic forcings. *Geophys. Res. Lett.*, **28**, 3317–3320.

Hu, Z.-Z., S. Yang, and R. Wu, 2003: Long-term climate variations in China and global warming signals. *J. Geophys. Res.*, **108**(D19), 4614, doi:10.1029/2003JD003651.

Huang, R., and Y. Wu, 1989: The influence of ENSO on the summer climate change in China and its mechanism. *Adv. Atmos. Sci.*, **6**, 21–32.

Huang, R., W. Chen, B. Yang, and R. Zhang, 2004: Recent advances in studies of the interaction between the East Asian winter and summer monsoons and ENSO cycle. *Adv. Atmos. Sci.*, **21**, 407–424.

Huffman, G. J., R. F. Adler, M. M. Morrissey, D. T. Bolvin, S. Curtis, R. Joyce, B. McGavock, and J. Susskind, 2001: Global precipitation at one-degree daily resolution from multisatellite observations. *Journal of Hydrometeorology*, **2**, 36–50.

IPCC, 2000: *Special Report on Emissions Scenarios*. N. Nakicenovic and R. Swart, Eds., Cambridge University Press, 612pp.

IPCC, 2001: *Climate Change 2001: The Scientific Basis. Contribution of Working Group I to the Third Assessment Report of the Intergovernmental Panel on Climate Change*. J. T. Houghton et al. Eds., Cambridge University Press, 881pp.

Kamiguchi, K., A. Kitoh, M. Hosaka, Y. Adachi, and Y. Murata, 2004: Evaluation of daily precipitation characteristics simulated by MRI-AGCM. *Proc. International Conf. on High-Impact Weather and Climate*, March 22–24, 2004, Seoul, Korea, 193–196.

Kawamura, R., 1998: A possible mechanism of the Asian summer monsoon-ENSO coupling. *J. Meteor. Soc. Japan,* **76**, 1009–1027.

Kharin, V. V., and F. W. Zwiers, 2000: Changes in the extremes in an ensemble of transient climate simulations with a coupled atmosphere-ocean GCM. *J. Climate*, **13**, 3760–3788.

Kitoh, A., S. Yukimoto, A. Noda, and T. Motoi, 1997: Simulated changes in the Asian summer monsoon at times of increased atmospheric CO_2. *J. Meteor. Soc. Japan*, **75**, 1019–1031.

Lal, M., and H. Harasawa, 2001: Future climate change scenarios for Asia as inferred from selected coupled atmosphere-ocean global climate models. *J. Meteor. Soc. Japan*, **79**, 219–227.

Min, S.-K., E.-H. Park, and W.-T. Kwon, 2004: Future projections of East Asian climate change from multi-AOGCM ensembles of IPCC SRES scenario simulations. *J. Meteor. Soc. Japan*, **82**, 1187–1211.

Nitta, T., and Z.-Z. Hu, 1996: Summer climate variability in China and its association with 500 hPa height and tropical convection. *J. Meteor. Soc. Japan,* **74**, 425–445.

Rajendran, K., A. Kitoh, and S. Yukimoto, 2004: South and East Asian summer monsoon climate and variation in the MRI coupled model (MRI-CGCM2). *J. Climate*, **17**, 763–782.

Semenov, V. A., and L. Bengtsson, 2002: Secular trends in daily precipitation characteristics: Greenhouse gas simulation with a coupled AOGCM. *Clim. Dyn.*, **19**, 123–140.

Watterson, I. G., and M. R. Dix, 2003: Simulated changes due to global warming in daily precipitation means and extremes and their interpretation using the gamma distribution. *J. Geophys. Res.*, **108**(D13), 4379, doi:10.1029/2002JD002928.

Xue, F., H. Wang, and J. He, 2004: Interannual variability of Mascarene High and Australian High and their influence on East Asian summer monsoon. *J. Meteor. Soc. Japan*, **82**, 1173–1186.

Yukimoto, S., and Coauthors, 2001: The new Meteorological Research Institute coupled GCM (MRI-CGCM2)-Model climate and variability. *Papers on Meteorology and Geophysics*, **51**, 47–88.

Zhang, R., A. Sumi, and M. Kimoto, 1996: Impact of El Niño on the East Asian monsoon: A diagnostic study of the ′86/87 and ′91/92 events. *J. Meteor. Soc. Japan*, **74**, 49–62.

Zwiers, F. W., and V. V. Kharin, 1998: Changes in the extremes of the climate simulated by CCC GCM2 under CO_2 doubling. *J. Climate*, **11**, 2200–2222.